Multibody Syst Dyn (2012) 28:257–282
DOI 10.1007/s11044-011-9300-9

Dynamic analysis of impact in swing-through crutch gait using impulsive and continuous contact models

Josep M. Font-Llagunes · Ana Barjau · Rosa Pàmies-Vilà · József Kövecses

Received: 17 June 2011 / Accepted: 29 December 2011 / Published online: 24 January 2012

Abstract The dynamics associated with the impact of the crutch with the ground is an important topic of research, since this is known to be the main cause of mechanical energy loss during swing-through gait. In this work, a multibody system representing a subject walking with crutches is used to investigate the behavior of two different contact models, impulsive and continuous, used for impact analysis. In the impulsive (discrete) approach, the impact interval is considered to be negligible and, therefore, the system configuration is constant. The postimpact state is directly obtained from the preimpact one through algebraic equations. In the continuous approach, the stiffness and dissipation characteristics of the contact surfaces are modeled through nonlinear springs and dampers. The equations of motion are integrated during the impact time interval to obtain the postimpact state, which, in principle, can differ from that obtained by means of the impulsive approach. Although both approaches have been widely used in the field of biomechanics, we have not found any comparative study in the existing literature justifying the model chosen for impact analysis. In this work, we present detailed numerical results and discussions to investigate several dynamic and energetic features associated with crutch impact. Based on the results, we compare the implications of using one contact model or the other.

Keywords Biomechanics · Human locomotion · Contact dynamics · Impact

J.M. Font-Llagunes (✉) · A. Barjau · R. Pàmies-Vilà
Department of Mechanical Engineering and Biomedical Engineering Research Centre, Universitat Politècnica de Catalunya, Diagonal 647, 08028 Barcelona, Catalunya, Spain
e-mail: josep.m.font@upc.edu

A. Barjau
e-mail: ana.barjau@upc.edu

R. Pàmies-Vilà
e-mail: rosa.pamies@upc.edu

J. Kövecses
Department of Mechanical Engineering and Centre for Intelligent Machines, McGill University, 817 Sherbrooke St. West, H3A 2K6 Montreal, Quebec, Canada
e-mail: jozsef.kovecses@mcgill.ca

1 Introduction

Crutch walking is a common type of gait among injured people, elderly people, sport-injured people, and even paraplegics. In their follow-up study of paraplegic individuals, Jaspers et al. [1] highlighted the psychological and physiological importance that paraplegics give to being able to stand and walk by themselves, something which can be achieved by means of crutch walking.

Crutch locomotion is much more demanding than normal walking. Different studies have shown that crutch walking is particularly demanding for the upper-body muscles which are not suited for such efforts [2–4]. Noreau et al. [2] found that the preferred speed and cadence in crutch walking are roughly 50% slower than in normal walking. Furthermore, the metabolic energy consumption (or metabolic cost) in crutch walking has been reported to be much higher than that of normal walking [5, 6]. Shoup et al. [7] measured joint displacements in the sagittal and frontal planes during crutch walking and compared their results with existing experimental data based on normal walking, and concluded that crutch design should try to minimize the vertical motion of the body and the impact associated to the crutch tip planting, as high contact forces on the crutch tip are transmitted to the upper limb joints causing damage. The excess effort associated with crutch walking may also lead to upper-limb joint degeneration [8], or even injuries in the nervous system like bilateral ulnar neuropraxia [9].

Both the high energy demand and the health risk associated with crutch walking have led scientists to develop dynamic analyses to better understand this type of locomotion. Model-based approaches have been widely used to study normal human walking, and have provided useful insight regarding the mechanical principles underlying human locomotion [10–12]. In [13], a model-based approach was presented to analyze the static stability of crutch-supported paraplegic standing for different values of hip-joint stiffness and crutch-to-feet distance. Nevertheless, as far as we know, little research has been done on model-based studies of the dynamics of the different phases of swing-through gait, that is, the first double support, the single support of crutches (and body swing-through), the second double support and the single support of legs. This is the most common type of gait for patients with low-thoracic or lumbar paraplegia [2].

This work proposes an anthropometric-based four-segmental model of the human body to analyze the impact of the crutch tip with the ground at the end of the single support of legs, and explores the two usual main approaches used to deal with impact problems: impulsive and continuous models [14, 15]. The use of one approach or the other depends on the purpose of the study. Surprisingly, no comparison has been found between the two approaches when applied to biomechanical systems. The aim of this paper is to fill this gap for the above mentioned crutch walking system.

In both methods, the beginning of contact is identified from geometric information, that is, when the crutch tip reaches the floor level at the end of crutch swing. As the crutch stays in contact with the ground after impact, the impact end corresponds to the compression end (i.e., the time when the crutch reaches zero normal velocity). A single-point contact model is accurate enough to study crutch tip contact. Thus, it is a suitable example to compare contact approaches. Other types of contact interactions appearing in biomechanical studies are more difficult to model accurately due to the complexity of the surfaces in contact and the difficulty in the identification of the mechanical characteristics of materials. Some examples for that are the foot-ground contact in human gait [16–18], the bone-to-bone contact at human body joints [19–21], or the contact between the lower limb and an external orthosis [22].

Impulsive formulations have been widely used for the analysis of passive dynamic walkers [23, 24] and bipedal systems [26, 27], and also to understand the physical principles of

human walking [11, 25] or running [28]. This methodology assumes that the contact interaction is instantaneous (compared to the time scale of the finite motion of the system) and, therefore, the system configuration is constant during the impact interval. In this case, the solution to the forward dynamics is achieved simply by solving a set of algebraic equations. Thus, only pre- and postimpact information is used in principle. This approach is very helpful to obtain performance indicators of the impact such as the mechanical energy loss or the magnitude of contact impulses [29, 30].

In continuous approaches, the duration of the contact transition is not considered instantaneous and so the configuration may change during the impact interaction. When contact is detected, contact forces are added to the differential equations of motion. This analysis requires a constitutive model explicitly representing the contact forces during impact as a function of the system state [31, 32]. An advantage of using continuous contact forces is that their time evolution can be traced during the impact interval, and thus an estimation of the maximum force occurring during the impact can be obtained. This is important in biomechanics because, as mentioned before, contact forces are transmitted to joints and are responsible for fatigue and joint damage. Compared to impulsive models, however, the use of continuous formulations results in a high computational cost since it requires the integration of the equations of motion. Moreover, a very small time step is needed due to the fast variation of forces and velocities within the impact interval. Another drawback is that such models require a characterization of both the geometry and the material properties of the bodies in contact in order to obtain suitable stiffness and damping parameters.

The energy loss, and the magnitude of the contact impulses and the postimpact velocities will be used as indicators to compare the performance of both contact formulations using the same preimpact states. We will analyze how the impact configuration and the model dynamic parameters influence the performance of the two contact models. These results can be interesting for crutch-use teaching in rehabilitation or for crutch design.

2 Dynamic model of the subject with crutches

We consider a patient with an injury at the lumbar region of the spinal cord who is able to perform a swing-through gait using crutches and knee-ankle-foot orthoses (KAFO). We assume that the patient has no motor control at the knee and ankle joints due to the injury. Therefore, the orthoses lock his knees to avoid flexion during leg support and constrain ankle plantar flexion to avoid foot drop. As a consequence, the patient's lower limb can be modeled as a single body segment.

The planar model of the subject with the crutches is shown in Fig. 1. It is composed of four segments (leg, torso, upper arm, and forearm plus crutch) linked by revolute joints modeling the hip, shoulder and elbow joints. Although there are two legs, two upper arms, and two forearms in the model, the segments will be named in singular throughout the text. We use a set of $n = 6$ independent generalized coordinates that form vector $\mathbf{q} = [q_1\ q_2\ q_3\ q_4\ q_5\ q_6]^T$, defined in Fig. 1. The first two correspond to the Cartesian coordinates of the foot P, the third one is the absolute orientation of the leg, and the remaining three correspond to the relative joint angles.

We assume that each segment is a rigid body and that the forearm and the crutch form a single segment. The length, the mass, the center of mass and the moment of inertia about it are respectively denoted by l_i, m_i, G_i, and I_i, $i = 1, 2, 3, 4$ (1-leg, 2-torso, 3-upper arm, 4-forearm plus crutch). Parameter a_i is the distance of G_i to the proximal joint (Fig. 1). The anthropometric data, summarized in Table 1, have been obtained according to [33] and

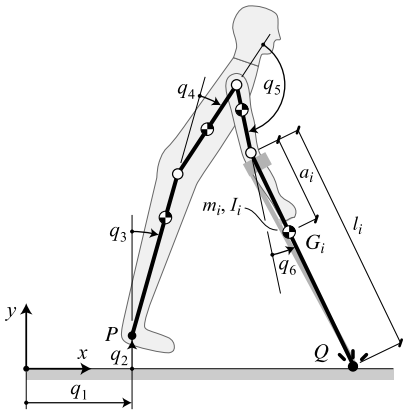

Fig. 1 Four-segmental model of the subject with crutches in the sagittal plane

Table 1 Anthropometric parameters of the model

	Leg	Torso	Upper arm	Forearm and crutch
m_i (kg)	22.54	40.46	3.92	4.28
I_i (kg·m^2)	2.07	2.66	0.044	0.433
l_i (m)	0.93	0.51	0.33	1.25
a_i (m)	0.42	0.34	0.14	0.33

assuming a total mass of 70 kg and a total height of 1.75 m. The two crutches have a mass of 1.2 kg and are 1 m long. We consider that the passive KAFO has a negligible weight as compared to leg's weight.

The starting point for the dynamics formulation (in both approaches) is the Lagrangian formalism

$$\mathbf{M}(\mathbf{q})\ddot{\mathbf{q}} + \mathbf{c}(\mathbf{q}, \dot{\mathbf{q}}) = \mathbf{f}_A + \mathbf{f}_C, \tag{1}$$

where $\mathbf{M}$ is the $n \times n$ mass or inertia matrix, $\mathbf{c}$ represents the $n \times 1$ array that contains inertial terms depending on position and velocities, and $\mathbf{f}_A$ and $\mathbf{f}_C$ stand for the $n \times 1$ arrays of generalized applied and contact forces, respectively. In this case, vector $\mathbf{f}_A$ is related to the net joint torques (at the hip, shoulder and elbow), and vector $\mathbf{f}_C$ is related to the contact forces (normal and tangential) that can appear at the foot P or the crutch tip Q. The formulations for both impulsive and continuous contact modeling are outlined in the subsequent sections.

3 Impulsive contact model

The impulsive model considers the impact interval to be very short in the characteristic time scale of the finite motion of the system, and the interaction is treated as a discrete event occurring during the continuous motion of the system. The configuration $\mathbf{q}$ is assumed to be constant during the "instantaneous" interaction, whereas velocities experience finite changes and accelerations reach infinite values. This latter fact is the reason for dealing with contact force impulses rather than with contact forces, and for using in principle the integrated form of the equations of motion, which are algebraic equations.

The main drawback in impulsive approaches is the detection of the collision end [34]. Neither the final state nor the final values of the impulses are in general known beforehand,

and an "end-of-collision criterion" has to be defined. Usually it is done through restitution coefficients (kinematic, kinetic or energetic) [15, 35] whose values vary within the interval $(0, 1)$. The kinematic and kinetic restitution coefficients may be in general energetically inconsistent whenever friction is not neglected and have to be used cautiously [34, 36].

The application example studied in this paper is that of a single-point impact with the ground in swing-through crutch gait. The study will be restricted to the sagittal plane, and so planar motion will be assumed from now on. In this particular case, as a new constraint is established on the crutch after impact (it has to remain in contact with the ground), the final normal velocity for the impact point Q has to be zero. This partial knowledge of the final state (as nothing is assumed regarding the final tangential velocity of Q) will allow in some cases the all-algebraic study of the collision without need of an energy dissipation assumption.

The velocity of the colliding point can be related to the generalized velocities through the $2 \times n$ Jacobian matrix $\mathbf{A}$: $\mathbf{v}(Q) = \mathbf{A}(\mathbf{q})\dot{\mathbf{q}}$. At impact configuration, the Jacobian matrix can be decomposed into two $1 \times n$ arrays specific for the normal and tangential components of $\mathbf{v}(Q)$

$$\mathbf{v}(Q) = \begin{Bmatrix} v_n(Q) \\ v_t(Q) \end{Bmatrix} = \begin{bmatrix} \mathbf{A}_n \\ \mathbf{A}_t \end{bmatrix} \dot{\mathbf{q}}. \tag{2}$$

The components v_n and v_t are positive when their direction is that of the positive y and x axis, respectively (Fig. 1). Denoting by t^- and t^+ the time instants just before and just after impact, respectively, the collision end condition can be written as

$$v_n^+(Q) = \mathbf{A}_n \dot{\mathbf{q}}^+ = 0, \tag{3}$$

which represents the new constraint condition of the system at postimpact time t^+. The impulsive approach used in this work starts with the general equations of motion, see (1). In our case, the only impulsive forces are the ground contact forces (both normal and tangential) at point Q. The inertial terms in $\mathbf{c}$ and the joint torques in $\mathbf{f}_A$ are essentially nonimpulsive. Thus, (1) becomes

$$\mathbf{M}\, d\dot{\mathbf{q}} = \mathbf{A}_n^T dP_n + \mathbf{A}_t^T dP_t \equiv \mathbf{A}^T \begin{Bmatrix} dP_n \\ dP_t \end{Bmatrix}, \tag{4}$$

where dP_n and dP_t are the differential normal and tangential contact impulses at Q. The total final impulses P_n^+ and P_t^+ can be obtained as

$$P_n^+ = \int_-^+ dP_n = \int_-^+ F_n(Q)\, dt, \qquad P_t^+ = \int_-^+ dP_t = \int_-^+ F_t(Q)\, dt, \tag{5}$$

where F_n and F_t are the normal and tangential contact forces at Q, respectively. The total normal impulse P_n^+ can never be negative (as F_n is always a repulsive force), whereas P_t^+ can have any sign (as $dP_t = F_t\, dt$ can be either positive or negative, according to the same sign criterion defined for v_t).

3.1 All-algebraic method

From (4), the postimpact velocities $\dot{\mathbf{q}}^+$ can be obtained formally from the preimpact ones $\dot{\mathbf{q}}^-$ as

$$\dot{\mathbf{q}}^+ = \dot{\mathbf{q}}^- + \mathbf{M}^{-1}\mathbf{A}^T \begin{Bmatrix} P_n^+ \\ P_t^+ \end{Bmatrix}. \tag{6}$$

Table 2 Different $v_t(Q)$ evolutions during impact in planar motion

Initial condition	$\mu < \mu_c$	$\mu \geq \mu_c$
$v_t^-(Q) = 0$	Immediate **permanent sliding**	**Permanent sticking**
$v_t^-(Q) \neq 0$	**Permanent sliding** or **sliding reversion**	**Permanent sliding** or **partial sliding** (sliding-sticking)

Combining this expression with (3) yields

$$0 = \mathbf{A}_n \dot{\mathbf{q}}^- + \left(\mathbf{A}_n \mathbf{M}^{-1} \mathbf{A}^T\right) \begin{Bmatrix} P_n^+ \\ P_t^+ \end{Bmatrix}. \tag{7}$$

This equation does not allow the calculation of the final impulses P_n^+ and P_t^+, directly from the initial state $\dot{\mathbf{q}}^-$, as $\mathbf{A}_n \mathbf{M}^{-1} \mathbf{A}^T$ is not invertible. Therefore, there is no general all-algebraic method giving the final state $\dot{\mathbf{q}}^+$ from the initial one $\dot{\mathbf{q}}^-$.

In planar motion, the end condition given by (3) can correspond to 4 different $v_t(Q)$ evolutions during the impact, according to the value of the friction coefficient μ and that of $v_t^-(Q)$. They are summarized in Table 2. For a rigorous justification, see [36, 37]. The critical value of the friction coefficient μ_c is given by

$$\mu_c = \left| \frac{\mathbf{A}_t \mathbf{M}^{-1} \mathbf{A}_n^T}{\mathbf{A}_t \mathbf{M}^{-1} \mathbf{A}_t^T} \right|, \tag{8}$$

and is configuration-dependent.

3.1.1 Permanent sticking and partial sliding

For the case of nonsliding end condition, regardless the sliding or nonsliding intermediate situations, the final state is given by

$$\mathbf{v}^+(Q) = \begin{Bmatrix} v_n^+(Q) \\ v_t^+(Q) \end{Bmatrix} = \mathbf{A} \dot{\mathbf{q}}^+ = \mathbf{0}. \tag{9}$$

This equation together with (7) yields

$$\begin{Bmatrix} P_n^+ \\ P_t^+ \end{Bmatrix} = -\left(\mathbf{A}\mathbf{M}^{-1}\mathbf{A}^T\right)^{-1} \mathbf{A} \dot{\mathbf{q}}^-. \tag{10}$$

The final velocities are then calculated by substituting back these final impulses into (6)

$$\dot{\mathbf{q}}^+ = \left[\mathbf{I} - \mathbf{M}^{-1}\mathbf{A}^T \left(\mathbf{A}\mathbf{M}^{-1}\mathbf{A}^T\right)^{-1} \mathbf{A}\right] \dot{\mathbf{q}}^-. \tag{11}$$

Using the projectors associated with the space of constrained and admissible motions, $\mathbf{H}_c$ and $\mathbf{H}_a$, respectively, defined in [29, 38]

$$\mathbf{H}_c = \mathbf{M}^{-1}\mathbf{A}^T \left(\mathbf{A}\mathbf{M}^{-1}\mathbf{A}^T\right)^{-1} \mathbf{A}, \tag{12}$$

$$\mathbf{H}_a = \mathbf{I} - \mathbf{H}_c = \mathbf{I} - \mathbf{M}^{-1}\mathbf{A}^T \left(\mathbf{A}\mathbf{M}^{-1}\mathbf{A}^T\right)^{-1} \mathbf{A}, \tag{13}$$

equation (11) can be expressed as

$$\dot{\mathbf{q}}^+ = (\mathbf{I} - \mathbf{H}_c) \dot{\mathbf{q}}^- = \mathbf{H}_a \dot{\mathbf{q}}^-. \tag{14}$$

The knowledge of the final state allows the calculation of the total change in kinetic energy but not that of the work associated to the normal and tangential impulses separately. However, this work (W_n^+ and W_t^+) can be calculated through the following integrals over the collision interval:

$$\begin{aligned} W_n^+ &= \int_-^+ v_n(Q)\, dP_n = \mathbf{A}_n \int_-^+ \dot{\mathbf{q}}\, dP_n \\ &= \mathbf{A}_n \int_-^+ \left[\dot{\mathbf{q}}^- + \mathbf{M}^{-1}\left(\mathbf{A}_n^T P_n + \mathbf{A}_t^T P_t\right)\right] dP_n \\ &= \mathbf{A}_n \dot{\mathbf{q}}^- P_n^+ + \left(\mathbf{A}_n \mathbf{M}^{-1} \mathbf{A}_n^T\right) \int_-^+ P_n\, dP_n + \left(\mathbf{A}_n \mathbf{M}^{-1} \mathbf{A}_t^T\right) \int_-^+ P_t\, dP_n, \end{aligned} \tag{15}$$

$$\begin{aligned} W_t^+ &= \int_-^+ v_t(Q)\, dP_t = \mathbf{A}_t \int_-^+ \dot{\mathbf{q}}\, dP_t \\ &= \mathbf{A}_t \int_-^+ \left[\dot{\mathbf{q}}^- + \mathbf{M}^{-1}\left(\mathbf{A}_n^T P_n + \mathbf{A}_t^T P_t\right)\right] dP_t \\ &= \mathbf{A}_t \dot{\mathbf{q}}^- P_t^+ + \left(\mathbf{A}_t \mathbf{M}^{-1} \mathbf{A}_n^T\right) \int_-^+ P_n\, dP_t + \left(\mathbf{A}_t \mathbf{M}^{-1} \mathbf{A}_t^T\right) \int_-^+ P_t\, dP_t. \end{aligned} \tag{16}$$

Though the total value of the integrals containing just P_n or just P_t can be obtained from the final impulses P_n^+ and P_t^+, the other ones require the knowledge of the evolution of one of them as a function of the other.

For the case of permanent sticking (which is more restrictive than just the nonsliding end condition), $v_t(Q) = 0$ throughout the whole collision, and so $\mathbf{A}_t\, d\dot{\mathbf{q}} = 0$. This leads to

$$dP_t = -\left(\mathbf{A}_t \mathbf{M}^{-1} \mathbf{A}_t^T\right)^{-1} \mathbf{A}_t \mathbf{M}^{-1} \mathbf{A}_n^T\, dP_n. \tag{17}$$

Substituting (17) back into (15) and (16) yields

$$W_n^+ = -\frac{1}{2} \mathbf{A}_n \mathbf{M}^{-1} \left[\mathbf{A}_n^T - \mathbf{A}_t^T \left(\mathbf{A}_t \mathbf{M}^{-1} \mathbf{A}_t^T\right)^{-1} \left(\mathbf{A}_t \mathbf{M}^{-1} \mathbf{A}_n^T\right)\right] \left(P_n^+\right)^2, \tag{18}$$

which equals the change in kinetic energy (energy loss) during impact (as the work related to the tangential impulse is obviously zero).

3.1.2 Permanent sliding with constant direction

When point Q slides, the tangential differential impulse dP_t has a direction opposite to the sliding velocity of point Q. If Coulomb's model is used to describe the friction phenomenon

$$dP_t = -\mu\sigma\, dP_n, \tag{19}$$

where $\sigma = \text{sign}[v_t(Q)]$ indicates the sliding direction ($\sigma = +1$ if Q slides along the positive x direction, and $\sigma = -1$ if it does along the negative one). Equation (4) becomes

$$\mathbf{M}\, d\dot{\mathbf{q}} = \left(\mathbf{A}_n^T - \mu \mathbf{A}_t^T \sigma\right) dP_n. \tag{20}$$

If the sliding direction is constant (as assumed in this case), vector $(\mathbf{A}_n^T - \mu \mathbf{A}_t^T \sigma)$ appearing in the previous equation is also constant, and the integration is straightforward yielding

$$\dot{\mathbf{q}}^+ = \dot{\mathbf{q}}^- + \mathbf{M}^{-1}\left(\mathbf{A}_n^T - \mu \mathbf{A}_t^T \sigma\right) P_n^+. \tag{21}$$

Using the condition given by (3) in (21), we obtain

$$P_n^+ = -\frac{\mathbf{A}_n}{\mathbf{A}_n \mathbf{M}^{-1}(\mathbf{A}_n^T - \mu \mathbf{A}_t^T \sigma)} \dot{\mathbf{q}}^-, \tag{22}$$

from which the final state can be calculated

$$\dot{\mathbf{q}}^+ = \left[\mathbf{I} - \frac{\mathbf{M}^{-1}(\mathbf{A}_n^T - \mu \mathbf{A}_t^T \sigma)\mathbf{A}_n}{\mathbf{A}_n \mathbf{M}^{-1}(\mathbf{A}_n^T - \mu \mathbf{A}_t^T \sigma)}\right] \dot{\mathbf{q}}^-. \tag{23}$$

The relationship between P_n and P_t given by (19) yields the following results for the work of the normal and tangential forces:

$$\begin{aligned} W_n^+ &= \mathbf{A}_n \dot{\mathbf{q}}^- P_n^+ + \frac{1}{2} \mathbf{A}_n \mathbf{M}^{-1} \big(\mathbf{A}_n^T - \mu \mathbf{A}_t^T \sigma\big)(P_n^+)^2 \\ &= -\frac{1}{2} \mathbf{A}_n \mathbf{M}^{-1} \big(\mathbf{A}_n^T - \mu \mathbf{A}_t^T \sigma\big)(P_n^+)^2, \end{aligned} \tag{24}$$

$$W_t^+ = -\mu \mathbf{A}_t \dot{\mathbf{q}}^- \sigma P_n^+ - \frac{1}{2} \mu \mathbf{A}_t \mathbf{M}^{-1} \big(\mathbf{A}_n^T - \mu \mathbf{A}_t^T \sigma\big) \sigma (P_n^+)^2. \tag{25}$$

3.1.3 Permanent sliding with reversion

The collision interval can be split into two subintervals: $[t^-, t^+] = [\sigma \ \textit{sliding}] + [-\sigma \ \textit{sliding}] = [t^-, t^i] + [t^i, t^+]$, where σ represents the initial sliding direction, that is, $\sigma = \text{sign}[v_t^-(Q)]$. The equations of motion for each subinterval can be integrated in a straightforward way. For the first subinterval,

$$\dot{\mathbf{q}}^i = \dot{\mathbf{q}}^- + \mathbf{M}^{-1} \big(\mathbf{A}_n^T - \mu \mathbf{A}_t^T \sigma\big) P_n^\sigma, \quad \mathbf{A}_t \dot{\mathbf{q}}^i = 0, \tag{26}$$

and for the second one

$$\dot{\mathbf{q}}^+ = \dot{\mathbf{q}}^i + \mathbf{M}^{-1} \big(\mathbf{A}_n^T + \mu \mathbf{A}_t^T \sigma\big) P_n^{-\sigma}, \quad \mathbf{A}_n \dot{\mathbf{q}}^+ = 0, \tag{27}$$

where $P_n^\sigma + P_n^{-\sigma} = P_n^+$. The solution of these equations yields

$$P_n^\sigma = \frac{-\mathbf{A}_t \dot{\mathbf{q}}^-}{\mathbf{A}_t \mathbf{M}^{-1}(\mathbf{A}_n^T - \mu \mathbf{A}_t^T \sigma)}, \tag{28}$$

$$P_n^{-\sigma} = \frac{-1}{\mathbf{A}_n \mathbf{M}^{-1}(\mathbf{A}_n^T + \mu \mathbf{A}_t^T \sigma)} \left[\mathbf{A}_n - \frac{\mathbf{A}_n \mathbf{M}^{-1}(\mathbf{A}_n^T - \mu \mathbf{A}_t^T \sigma)\mathbf{A}_t}{\mathbf{A}_t \mathbf{M}^{-1}(\mathbf{A}_n^T - \mu \mathbf{A}_t^T \sigma)}\right] \dot{\mathbf{q}}^-, \tag{29}$$

and the postimpact velocities $\dot{\mathbf{q}}^+$ result

$$\dot{\mathbf{q}}^+ = \dot{\mathbf{q}}^- + \mathbf{M}^{-1} \big(\mathbf{A}_n^T - \mu \mathbf{A}_t^T \sigma\big) P_n^\sigma + \mathbf{M}^{-1} \big(\mathbf{A}_n^T + \mu \mathbf{A}_t^T \sigma\big) P_n^{-\sigma}. \tag{30}$$

Knowing the values of the partial normal impulses P_n^{σ} and $P_n^{-\sigma}$ allows the calculation of the work associated with the normal and tangential impulses separately:

$$\begin{aligned} W_n^+ &= \int_-^i v_n(Q)\,dP_n + \int_i^+ v_n(Q)\,dP_n \\ &= \mathbf{A}_n \int_-^i \left[\dot{\mathbf{q}}^- + \mathbf{M}^{-1}\left(\mathbf{A}_n^T - \mu \mathbf{A}_t^T \sigma\right) P_n\right] dP_n \\ &\quad + \mathbf{A}_n \int_i^+ \left[\dot{\mathbf{q}}^i + \mathbf{M}^{-1}\left(\mathbf{A}_n^T + \mu \mathbf{A}_t^T \sigma\right) P_n\right] dP_n \\ &= \mathbf{A}_n\left(\dot{\mathbf{q}}^- P_n^{\sigma} + \dot{\mathbf{q}}^i P_n^{-\sigma}\right) \\ &\quad + \frac{1}{2}\mathbf{A}_n \mathbf{M}^{-1}\left[\left(\mathbf{A}_n^T - \mu \mathbf{A}_t^T \sigma\right)\left(P_n^{\sigma}\right)^2 + \left(\mathbf{A}_n^T + \mu \mathbf{A}_t^T \sigma\right)(P_n^{-\sigma})^2\right], \end{aligned} \tag{31}$$

$$\begin{aligned} W_t^+ &= \int_-^i v_t(Q)\,dP_t + \int_i^+ v_t(Q)\,dP_t \\ &= \mathbf{A}_t \int_-^i \left[\dot{\mathbf{q}}^- + \mathbf{M}^{-1}\left(\mathbf{A}_n^T - \mu \mathbf{A}_t^T \sigma\right) P_n\right] dP_t \\ &\quad + \mathbf{A}_t \int_i^+ \left[\dot{\mathbf{q}}^i + \mathbf{M}^{-1}\left(\mathbf{A}_n^T + \mu \mathbf{A}_t^T \sigma\right) P_n\right] dP_t \\ &= -\mu \mathbf{A}_t\left(\dot{\mathbf{q}}^- \sigma P_n^{\sigma}\right) \\ &\quad - \frac{1}{2}\mu \mathbf{A}_t \mathbf{M}^{-1}\left[\left(\mathbf{A}_n^T - \mu \mathbf{A}_t^T \sigma\right)(P_n^{\sigma})^2 - \left(\mathbf{A}_n^T + \mu \mathbf{A}_t^T \sigma\right)(P_n^{-\sigma})^2\right]\sigma. \end{aligned} \tag{32}$$

For the particular case $\sigma = +1$, equation (32) simplifies into

$$W_t^+ = -\mu \mathbf{A}_t\left(\dot{\mathbf{q}}^- P_n^{\sigma}\right) - \frac{1}{2}\mu \mathbf{A}_t \mathbf{M}^{-1}\left[\left(\mathbf{A}_n^T - \mu \mathbf{A}_t^T\right)\left(P_n^{\sigma}\right)^2 - \left(\mathbf{A}_n^T + \mu \mathbf{A}_t^T\right)(P_n^{-\sigma})^2\right]. \tag{33}$$

If $\sigma = -1$, then

$$W_t^+ = +\mu \mathbf{A}_t\left(\dot{\mathbf{q}}^- P_n^{\sigma}\right) + \frac{1}{2}\mu \mathbf{A}_t \mathbf{M}^{-1}\left[\left(\mathbf{A}_n^T + \mu \mathbf{A}_t^T\right)(P_n^{\sigma})^2 - \left(\mathbf{A}_n^T - \mu \mathbf{A}_t^T\right)\left(P_n^{-\sigma}\right)^2\right]. \tag{34}$$

3.2 Integrative method

The analytical solutions presented above do not give any information about the time history of normal and tangential forces at Q, the time history of their associated work W_n and W_t, and the evolution of $\mathbf{v}(Q)$ during the impact, as time is not a variable in that formulation.

However, the analyses presented in Sect. 3.1 suggest the possibility of using P_n as independent variable to trace those evolutions for the two particular cases of permanent nonsliding (sticking) and permanent sliding conditions. This may give more information to compare with the results obtained with the continuous model.

Once the final value of the normal impulse P_n^+ has been obtained, a regular P_n differential can be defined (for instance, $dP_n = P_n^+/10^3$) and the P_n-dependent evolution of the other variables can be explored.

In order to compare the evolution of variables obtained with the two approaches, it will be necessary to establish a suitable equivalence between the independent variables (P_n and t),

as in principle there is not a simple proportionality between the P_n scale in the impulsive approach and the time scale in the continuous one.

4 Continuous contact model

The continuous contact models, also referred to as "compliant" or "penalty" models, take into account the finite duration of the impact phase. These techniques relax the contact constraints and replace them with constitutive relations establishing an explicit representation of the contact forces as a function of the system state. The associated generalized forces $\mathbf{f}_C$ appear on the right-hand side of (1). In this approach, the required model parameters, associated with the geometry of the surfaces in contact and materials mechanical characteristics, are not always easy to identify.

4.1 Normal force model

The simplest continuous formulations for the normal force are the Maxwell and the Kelvin–Voigt models [15, 39], where this force is represented through a series or parallel linear spring-damper element, respectively. They have been widely used due to their simplicity. However, nonlinearity is an essential feature of impact problems [41]. In this work, we use a nonlinear Hunt–Crossley model to account for the nonlinear relationship between normal contact force and indentation of the colliding point [40–44]. For the case of single-point contact of spherical surfaces, Hunt and Crossley [40] propose the following expression for the normal contact force F_n:

$$F_n = k_n |\delta_n|^{\frac{3}{2}} + \chi |\delta_n|^{\frac{3}{2}} \dot{\delta}_n, \tag{35}$$

where k_n is the generalized normal stiffness according to Hertz theory [45] (depending on the mechanical properties of the materials and the surfaces curvature), δ_n (>0) and $\dot{\delta}_n$ are the normal indentation between bodies and its time derivative, and χ is the hysteresis damping factor. In this paper, the contacts are modeled as sphere-to-plane. Thus, the generalized stiffness k_n can be calculated as [15, 45]

$$k_n = \frac{4E^* \sqrt{R_s}}{3}, \tag{36}$$

where R_s is the radius of the sphere and E^* is the effective Young's modulus, which can in turn be calculated through

$$E^* = \left[\frac{1 - \nu_s^2}{E_s} + \frac{1 - \nu_p^2}{E_p} \right]^{-1}. \tag{37}$$

E_s and E_p stand for the Young's modulus of the materials of the sphere and the plane, and ν_s and ν_p stand for the Poisson's ratio of the same materials.

4.2 Tangential force model

The tangential contact force F_t is described through the Coulomb dry friction model. The tangential force is treated as an unknown of the problem when there is no relative tangential velocity between the bodies in contact. In that case, the condition is that $|F_t| \leq \mu_s F_n$, where

μ_s is the static coefficient of friction. When that condition is broken or a relative tangential velocity between the bodies in contact appears, the tangential force is formulated as

$$F_t = -\mu\sigma F_n, \tag{38}$$

where μ is the dynamic coefficient of friction. For the sake of simplicity, in this study, we assume $\mu_s = \mu$.

5 Results and discussion

The postimpact velocities of the foot and crutch contact points, as well as the normal and tangential impulses and their associated work, have been obtained with both the impulsive and the continuous approaches for a wide set of initial states and friction coefficients. These results are a step further compared to the ones presented in a previous work [30], which were obtained just with an impulsive approach assuming permanent nonsliding condition at the impact point. The preimpact state $(\mathbf{q}^-, \dot{\mathbf{q}}^-)$ is defined according to kinematic studies of subjects walking with crutches [2]. The absolute angle for the back leg, q_3^-, has been varied between 3° and 21° with a step of 3°. The other ones have been taken constant ($q_4^- = 10°$, $q_5^- = 150°$) except for the last one, q_6^-, which has been adjusted systematically to guarantee ground contact at the crutch tip. Figure 2 shows the seven chosen configurations. The whole aspect of the system can be described as going from a rather upright configuration to one with the body leaning forward.

Concerning preimpact velocities, kinematic studies show that relative angular velocities associated with the hip, shoulder, and elbow joints are approximately zero before crutch tip impact [2]. In this study, the preimpact angular velocity of the back leg $\dot{q}_3^-$ is taken equal to 1 rad/s (though it may have other values depending on the subject specific pathology). This angular velocity is related to an ankle rotation in the dorsiflexion direction. The preimpact angular velocities associated with the hip and elbow joints, $\dot{q}_4^-$ and $\dot{q}_6^-$, are assumed to be zero in all simulations. Finally, the shoulder joint angular velocity, $\dot{q}_5^-$, has been varied uniformly between -0.2 rad/s and $+0.4$ rad/s in order to obtain different initial tangential velocities at the contact point Q. The minimum and maximum values for the normal and tangential components of the colliding point preimpact velocity, $\mathbf{v}^-(Q)$, are given on Fig. 2. For the sake of conciseness, only a set of representative results will be presented.

The explored configurations lead to seven different values for the critical friction coefficient, see (8), which are plotted in Fig. 3. This information is useful in order to choose appropriate values covering all the different possibilities summarized in Table 2. We have decided to work with $\mu = 1$ (above all the critical values μ_c), $\mu = 0.5$ (lower than all the μ_c), and an intermediate value of $\mu = 0.75$ (higher than the first five μ_c and lower than the last two μ_c). These three values are indicated in Fig. 3 with dotted red lines.

The nominal parameters used in the normal force model are the following: $R_s = 0.05$ m, $E_s = 0.1 \cdot 10^9$ Pa, $\nu_s = 0.5$ for the crutch tip elastomeric material; and $E_p = 30 \cdot 10^9$ Pa, $\nu_p = 0.2$ for the planar floor which is considered to be concrete. The hysteresis damping factor χ is taken equal to 10^7 N s/m$^{2.5}$. A sensitivity analysis to parameters k_n, see (36), and χ is presented in Sect. 5.5.

Besides the fact that the impulsive treatment is a "frozen time" one, the two approaches differ essentially on the treatment of the normal forces, but not on that of the tangential ones. While the latter are modeled as Coulomb's dry friction phenomena (that is, proportional to the normal reaction forces through the friction coefficient μ), the former are not modeled in

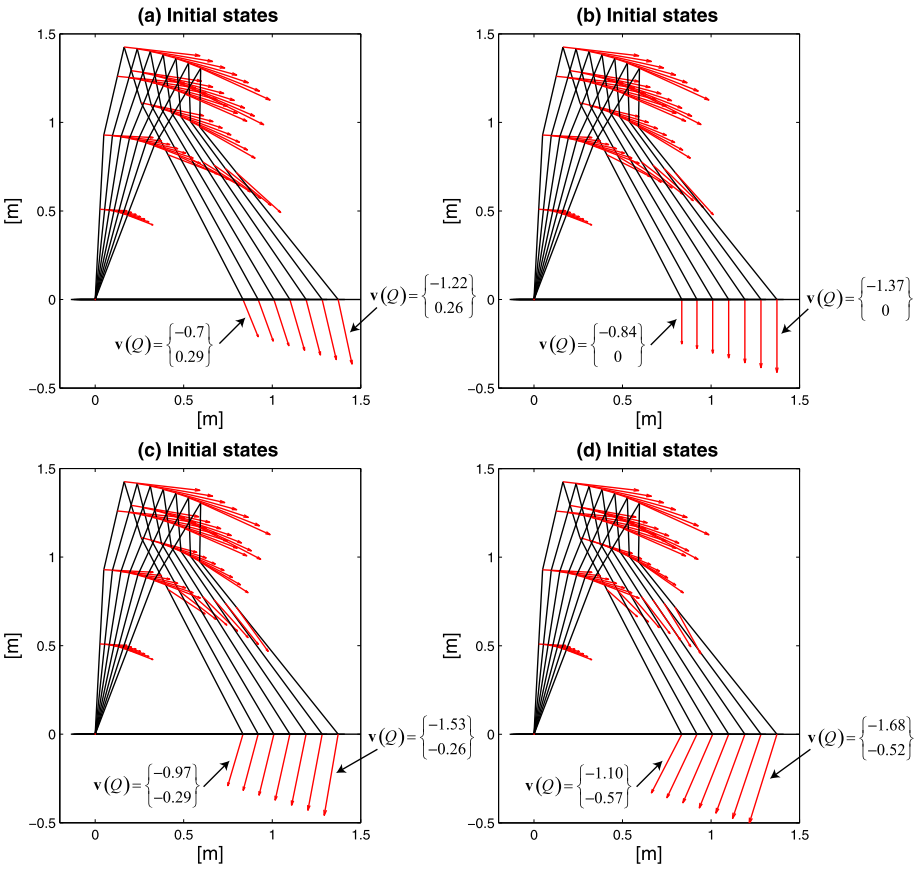

Fig. 2 Initial states of the subject with crutches used in the simulations. The components of $\mathbf{v}(Q)$ are as defined in (2): $\mathbf{v}(Q) = \{v_n(Q), v_t(Q)\}^T$ (in m/s). (**a**) $\dot{q}_5 = -0.2$ rad/s, (**b**) $\dot{q}_5 = 0$, (**c**) $\dot{q}_5 = +0.2$ rad/s, (**d**) $\dot{q}_5 = +0.4$ rad/s

the impulsive method (only their impulses are considered). In the continuous method, they are modeled through (35). However, in both approaches, the collision end corresponds to the same kinematic condition expressed in (3) (zero final normal velocity of the crutch tip).

Another difference between the two approaches comes from the treatment of the applied forces in (1), which are related to net joint torques. It was said that in the impulsive approach those forces do not play any role because they are essentially nonimpulsive. However, they do have to be considered in a continuous simulation. Noreau et al. [2] presented torque patterns at the hip, shoulder and elbow for nondisabled and paraplegic individuals along the swing-through gait cycle. The crutch impact corresponds to the 100% of the cycle. From the results and comments in [2], it can be concluded that hip torques are very low in paraplegic subjects, due to the poor activation of hip muscles. Furthermore, the hip moment is very close to zero at the instant of crutch impact. Regarding the upper limb joint torques, it is clearly visible that the crutch stance phase is highly demanding for the involved muscles, whereas the crutch swing involves less muscle activity. In fact, both shoulder and elbow torques are approximately zero at crutch impact. For the mentioned reasons, all the joint torques are assumed to be zero in the simulations.

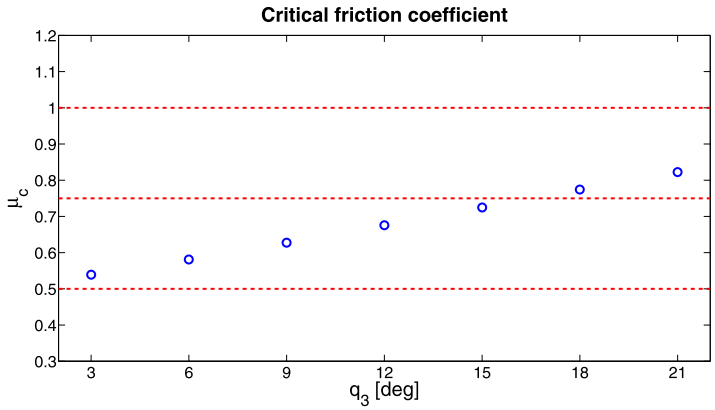

Fig. 3 Critical friction coefficient (μ_c) as a function of the leg absolute angle (q_3)

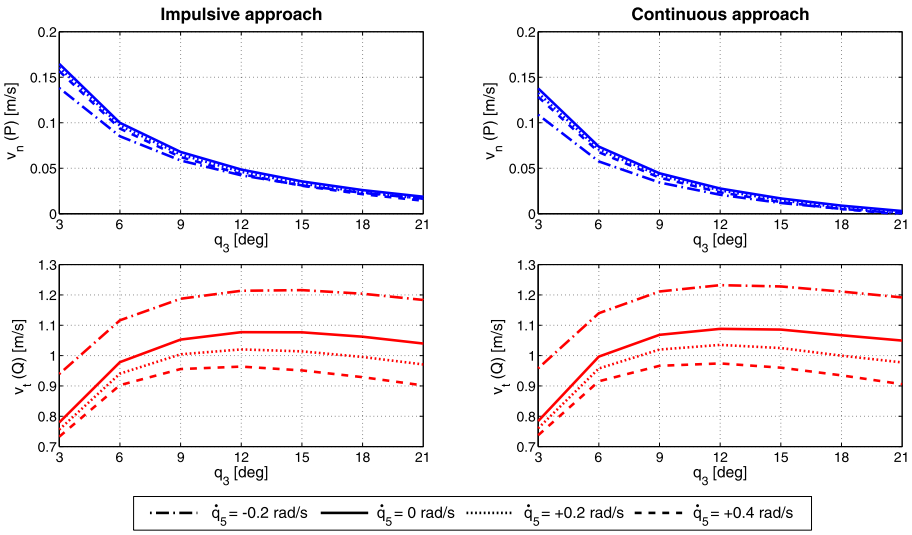

Fig. 4 Postimpact velocities as a function of the leg absolute angle (q_3) for $\mu = 0.5$ and different initial values of $\dot{q}_5$

5.1 Kinematic analysis

Figures 4, 5, and 6 correspond to the three different values of friction coefficients ($\mu = 0.5$, $\mu = 0.75$, and $\mu = 1$, respectively) used in the simulations. The plotted variables are the postimpact values of the normal foot velocity, $v_n^+(P)$, and the tangential crutch velocity, $v_t^+(Q)$, as a function of coordinate q_3. The curves correspond to different initial values of $\dot{q}_5$ (from -0.2 rad/s to $+0.4$ rad/s). These curves show that the two approaches yield very similar kinematic results. Furthermore, the shape of the curves for different body configurations is also very close.

Two particular features deserve a comment. First of all, it is clear that walking with an upright configuration (low angle q_3^-) facilitates the foot push-off because the normal

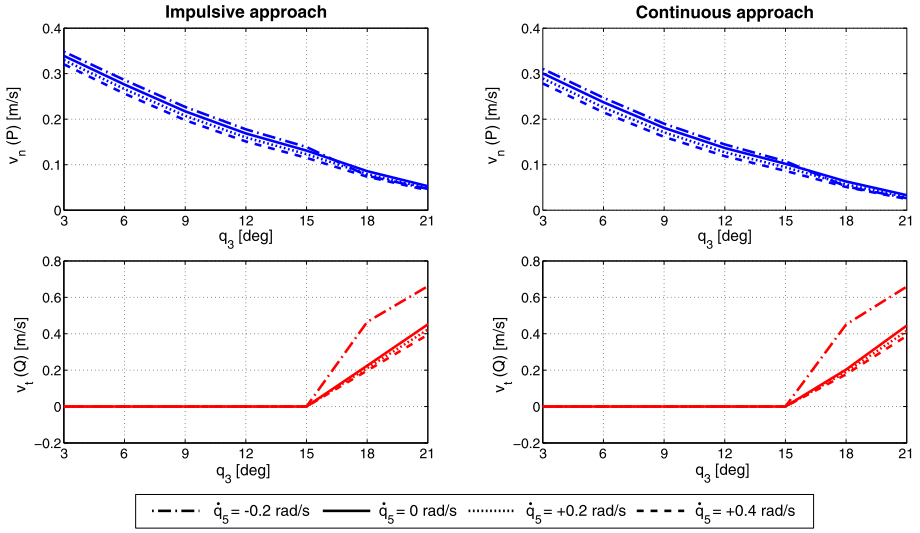

Fig. 5 Postimpact velocities as a function of the leg absolute angle (q_3) for $\mu = 0.75$ and different initial values of $\dot{q}_5$

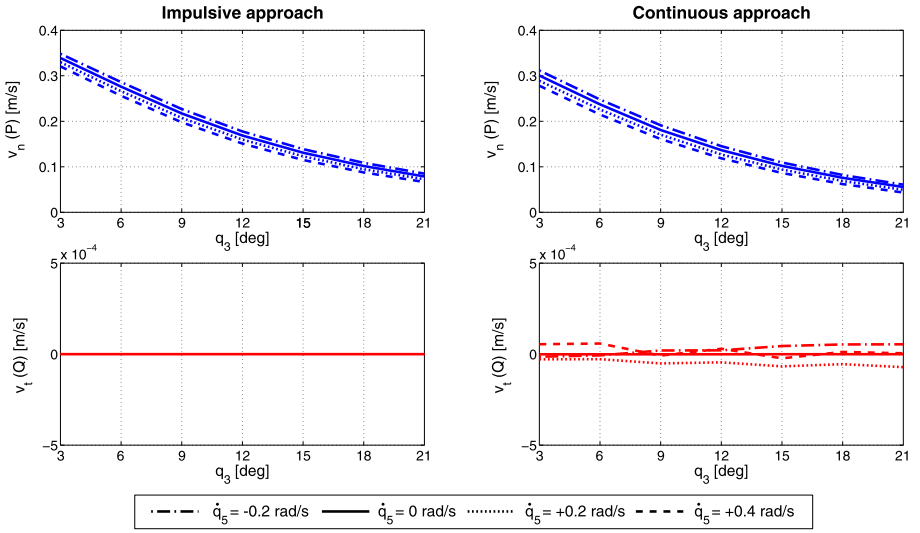

Fig. 6 Postimpact velocities as a function of the leg absolute angle (q_3) for $\mu = 1$ and different initial values of $\dot{q}_5$

postimpact velocity of the foot increases. Secondly, in all cases with $\mu = 0.75$ the upright configuration is also advisable in order to avoid sliding (Fig. 5). This is because for those configurations the critical friction coefficient μ_c is lower, according to Fig. 3. The final values of the crutch tip tangential velocity are consistent with the expected behavior according to the friction coefficient value:

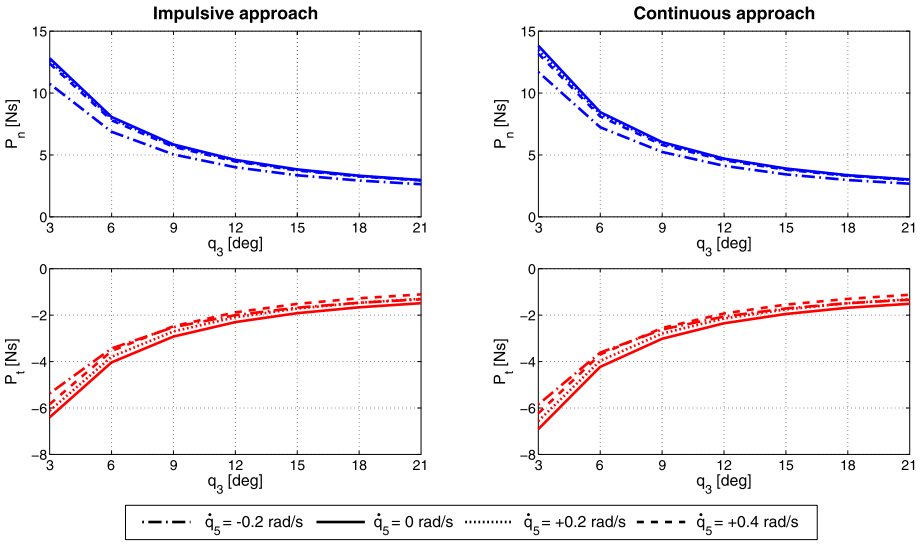

Fig. 7 Contact impulses (P_n^+, P_t^+) as a function of the leg absolute angle (q_3) for $\mu = 0.5$ and different initial values of $\dot{q}_5$

- For $\mu = 0.5$, as this value lies under all the critical values shown in Fig. 3, sliding is guaranteed from the very beginning regardless the initial $v_t^-(Q)$ value. The sliding condition $v_t(Q) \neq 0$ is kept all over the impact interval.
- For $\mu = 0.75$, sticking is possible only for the configurations from $q_3^- = 3°$ to $q_3^- = 15°$. Of course, sticking is not guaranteed as it depends on the initial tangential velocity of the crutch tip. The higher the $v_t^-(Q)$ value, the later sticking will start. Eventually, for really high values of $v_t^-(Q)$, sticking may not happen. In the cases depicted on Fig. 5, the sticking state is reached in all simulations with $q_3^- \leq 15°$.
- For $\mu = 1$, sticking is possible for all configurations, but it is not guaranteed for the same aforementioned reasons. However, Fig. 6 shows that the sticking state is reached in all the simulated cases.

Final values of $v_t^+(Q)$ are not enough to prove the constant sliding for $\mu = 0.5$. The step-by-step evolution within the collision process has to be explored. As the impulsive approach is a "frozen-time" one, this evolution is explored as a function of the normal impulse. This can also be done in the continuous approach, as the time-evolution of the normal impulse $P_n(t)$ is one of the results. This will be explored in Sect. 5.4.

5.2 Dynamic analysis

Figures 7, 8, and 9 show the postimpact values of the normal and tangential impulses developed at the crutch tip, P_n^+ and P_t^+, as a function of q_3^-, and for the same μ and $\dot{q}_5^-$ values. Again, the results obtained by means of the two approaches are really similar. It is important to note that in the continuous approach the impulses are not directly obtained (as in the impulsive one), but they can be calculated by numerical time integration of the contact forces (F_n and F_t) over the whole impact interval. A trapezoidal integration method was used for this purpose.

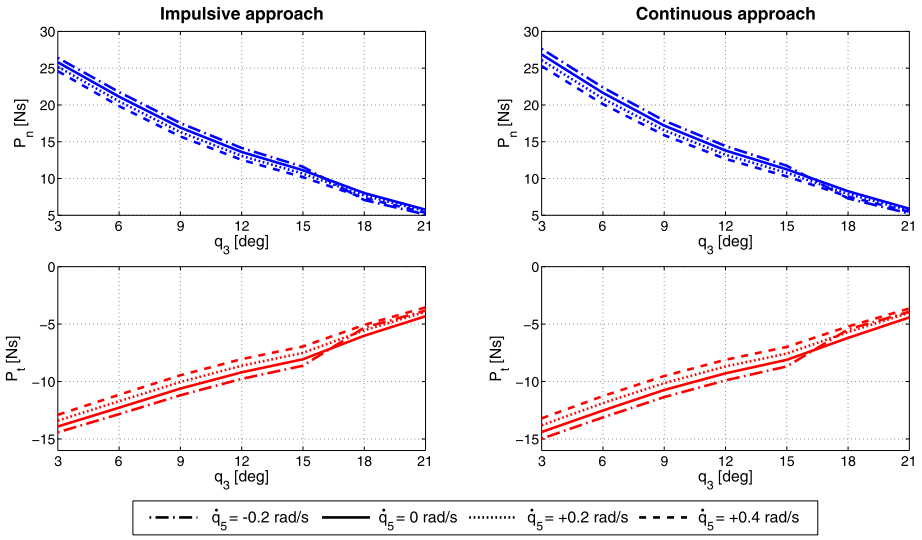

Fig. 8 Contact impulses (P_n^+, P_t^+) as a function of the leg absolute angle (q_3) for $\mu = 0.75$ and different initial values of $\dot{q}_5$

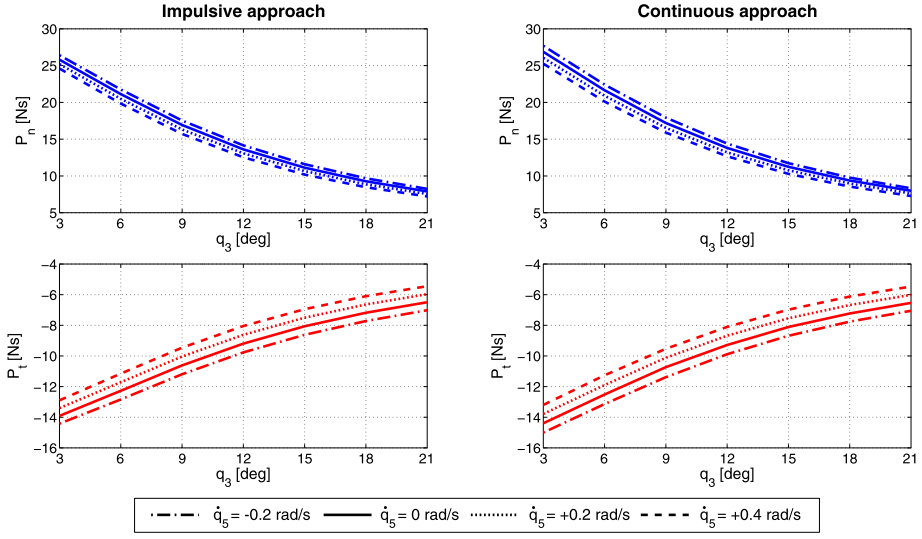

Fig. 9 Contact impulses (P_n^+, P_t^+) as a function of the leg absolute angle (q_3) for $\mu = 1$ and different initial values of $\dot{q}_5$

Comparison between $v_n^+(P)$ (Figs. 4, 5, and 6) and P_n^+ (Figs. 7, 8, and 9) shows a clear correlation between these postimpact values: the higher the normal impulse is, the higher the normal foot velocities will be after impact.

Concerning the tangential impulse, its value is negative in all cases regardless the initial $v_t^-(Q)$ direction. It must be pointed out that both P_n^+ and P_t^+ increase in absolute value for upright configurations (low value of q_3^-), therefore, higher impulses at the crutch tip are

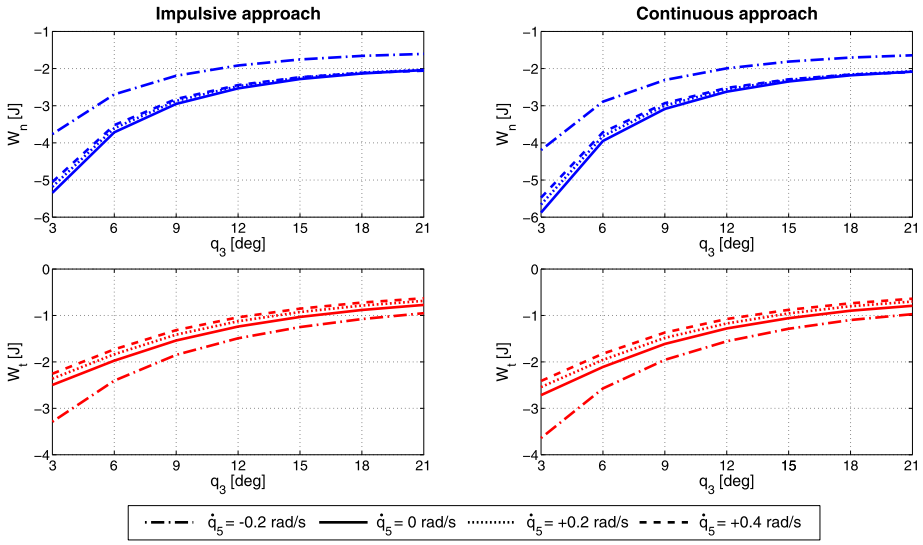

Fig. 10 Work of the normal and tangential forces (W_n^+, W_t^+) as a function of the leg absolute angle (q_3) for $\mu = 0.5$ and different initial values of $\dot{q}_5$

developed for those body postures. It must be kept in mind that high contact forces acting on the crutch tip are transmitted to upper limb joints and may cause their damage [8], or even injuries in the nervous system [9].

5.3 Energy analysis

Figures 10, 11, and 12 show the work of the normal and tangential forces, W_n^+ and W_t^+, as function of q_3^-, and for the same μ and $\dot{q}_5^-$ values.

In the impulsive approach, the total of the work of these two force components equals the kinetic energy change (which is obviously negative due to the impact loss):

$$\Delta T = T^+ - T^- = W_n^+ + W_t^+. \tag{39}$$

In the continuous approach, however, (39) is not rigorously true (because the configuration is allowed to change and the potential energy may vary) but it represents a very good estimation of the kinetic energy loss. Mechanical work balances are interesting to assess the energy loss associated to the crutch impact. Though a lower loss implies (in principle) a lower metabolic cost, this cannot be taken as the good criterion to choose the "best" performance: for example, when sliding, a high energy loss is advisable in order to evolve to a sticking phase.

Comparison between P_n^+ (Figs. 7, 8, and 9) and W_n^+ (Figs. 10, 11, and 12) shows a clear correlation between these postimpact values: the higher the normal impulse is, the higher the absolute value of its work $|W_n^+|$ becomes.

The $|W_n^+|$ value is in general larger than that of $|W_t^+|$. For a same μ value, the different initial velocities do not play a significant role, whereas the configuration does have an effect: changing from the upright configuration to the leaning one may imply a reduction in the magnitude of the normal work of more than 50%.

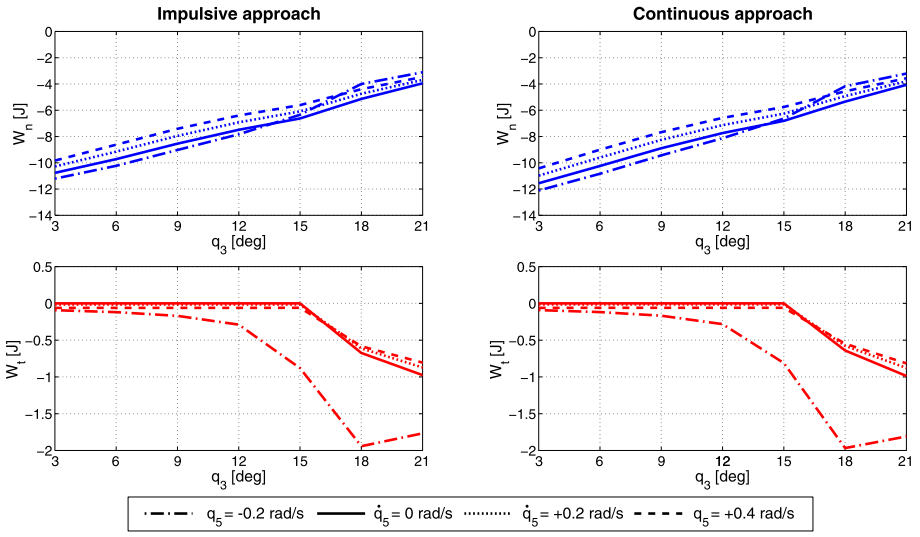

Fig. 11 Work of the normal and tangential forces (W_n^+, W_t^+) as a function of the leg absolute angle (q_3) for $\mu = 0.75$ and different initial values of $\dot{q}_5$

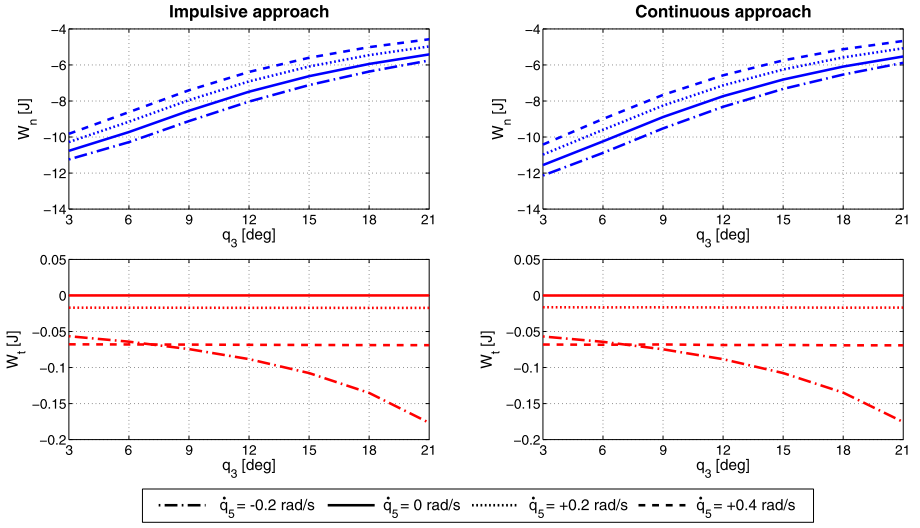

Fig. 12 Work of the normal and tangential forces (W_n^+, W_t^+) as a function of the leg absolute angle (q_3) for $\mu = 1$ and different initial values of $\dot{q}_5$

The work of the tangential force, W_t^+, is zero for nonsliding cases (though $P_t^+ \neq 0$ for those cases), and the energy loss is only due to the work associated with the normal impulse. As seen in Figs. 10, 11, and 12, when sliding occurs the work of the tangential force increases in magnitude when increasing the leaning posture, but its value is always well below that of the normal one. The only exception to that tendency corresponds to the lowest friction coefficient ($\mu = 0.5$).

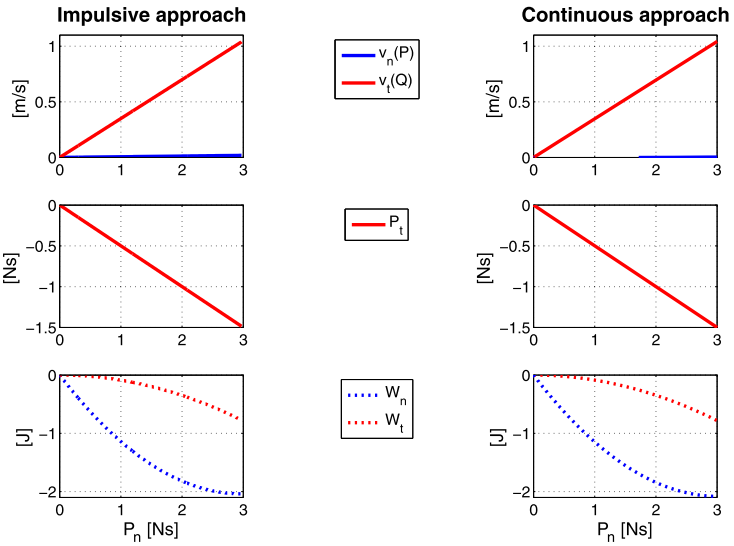

Fig. 13 Evolution of $v_n(P)$, $v_t(Q)$, P_t, W_n, W_t as a function of the normal impulse P_n. Case: $\mu = 0.5$, $\dot{q}_5^- = 0$, $q_3^- = 21°$ (Immediate sliding)

5.4 Evolution of variables as function of the normal impulse P_n

Figures 13 to 17 show the evolution, as a function of the normal impulse P_n, of the kinematic, dynamic and energy quantities explored in the previous subsections ($v_n(P)$, $v_t(Q)$, P_t, W_n, W_t). Only the results for two values of the friction coefficient μ ($\mu = 0.5, 0.75$) are shown. The initial values for q_3 have been varied between 3° and 21°, and between -0.2 rad/s and $+0.4$ rad/s for the initial $\dot{q}_5$.

The results obtained with the two approaches are extremely close for the case $\mu = 0.5$. For $\mu = 0.75$, there are only nonnegligible discrepancies in the final normal foot velocity $v_n(P)$ values. They are systematically higher (up to 10%) in the impulsive approach than in the continuous one.

Other interesting features deserve a comment. Figures 13 and 14 were obtained with the same friction coefficient ($\mu = 0.5$) and initial configuration ($q_3 = 21°$). In both cases, we are below the critical value ($\mu < \mu_c$). Thus, crutch sliding is guaranteed from the very beginning, even if its initial tangential velocity $v_t^-(Q)$ is zero (as is the case in Fig. 13). In Fig. 14, $v_t^-(Q) < 0$ but an instantaneous nonsliding condition is reached shortly after. However, it cannot be maintained and sliding restarts immediately in the opposite direction (in other words, there is sliding reversion).

Figures 15, 16, and 17 correspond to $\mu = 0.75$. In Fig. 15, the initial configuration is $q_3 = 12°$, and so the friction value is clearly above the critical one ($\mu > \mu_c$). In that case, if the sticking state is attained ($v_t(Q) = 0$), it will be maintained until the impact end. This is precisely the case shown in Fig. 15: though the initial tangential velocity for the crutch tip is $v_t^-(Q) < 0$, the sliding phase is followed by a sticking one.

In the other two cases (Figs. 16 and 17), the initial configuration is such that the friction coefficient lies slightly above and slightly below the critical value, respectively. In both cases the crutch is not sliding initially. In Fig. 16, the sticking state is kept all over the impact, whereas immediate sliding appears in Fig. 17, as expected.

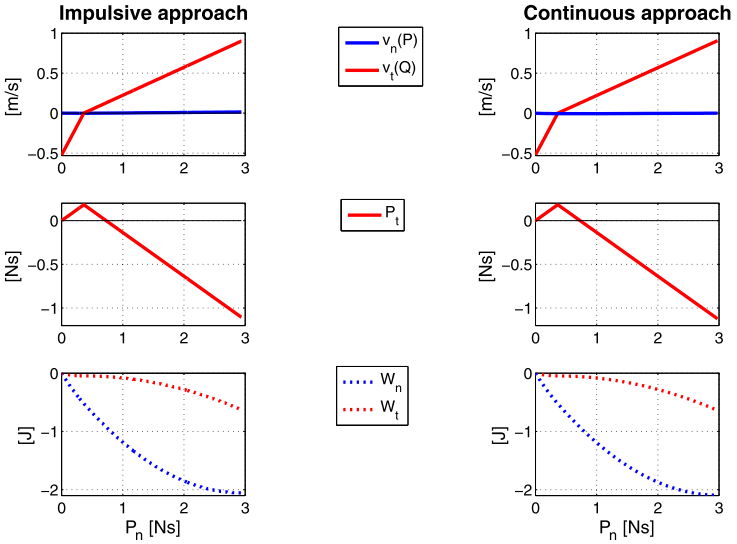

Fig. 14 Evolution of $v_n(P)$, $v_t(Q)$, P_t, W_n, W_t as a function of the normal impulse P_n. Case: $\mu = 0.5$, $\dot{q}_5^- = 0.4$ rad/s, $q_3^- = 21°$ (Sliding reversion)

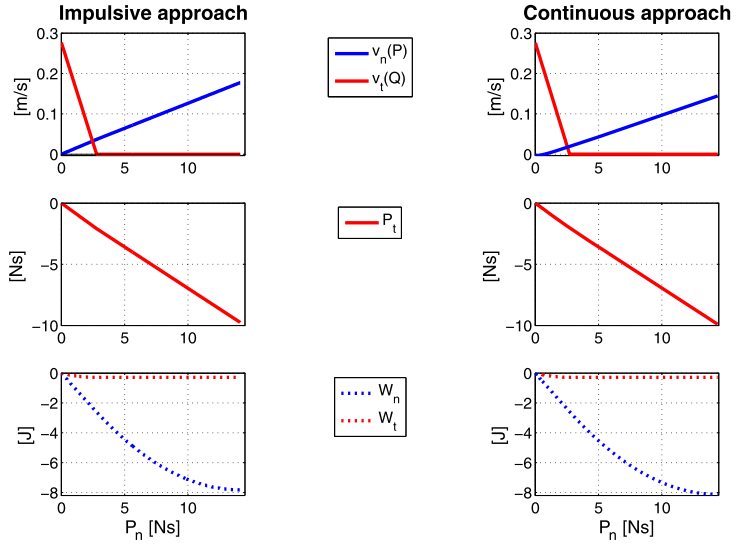

Fig. 15 Evolution of $v_n(P)$, $v_t(Q)$, P_t, W_n, W_t as a function of the normal impulse P_n. Case: $\mu = 0.75$, $\dot{q}_5^- = -0.2$ rad/s, $q_3^- = 12°$ (Sliding-sticking)

5.5 Sensitivity of the continuous approach to parameters k_n and χ

Different values of the continuous model parameters k_n and χ result in different time evolution of the kinematics and dynamics during the impact interval. For instance, low values of k_n increase the impact duration and reduce the peak values of the contact forces. However,

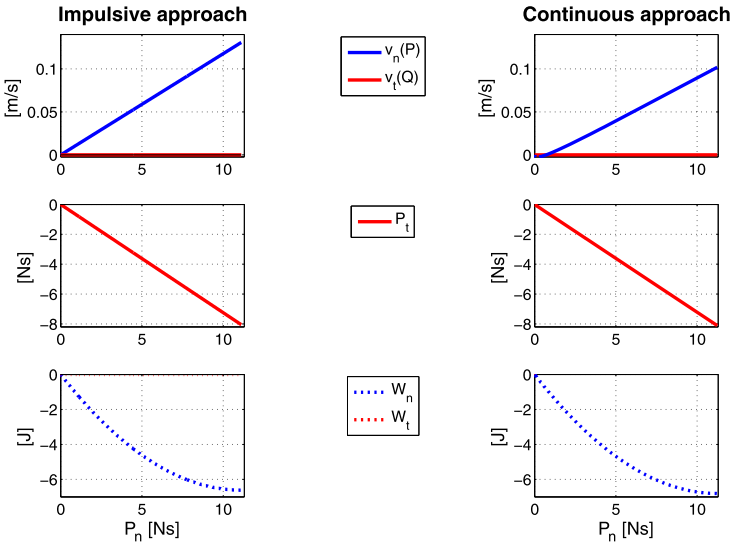

Fig. 16 Evolution of $v_n(P)$, $v_t(Q)$, P_t, W_n, W_t as a function of the normal impulse P_n. Case: $\mu = 0.75$, $\dot{q}_5^- = 0$, $q_3^- = 15°$ (Permanent sticking)

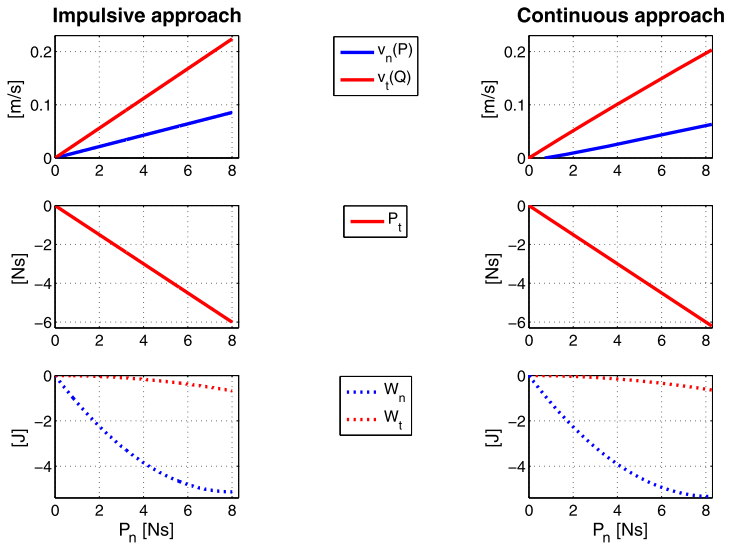

Fig. 17 Evolution of $v_n(P)$, $v_t(Q)$, P_t, W_n, W_t as a function of the normal impulse P_n. Case: $\mu = 0.75$, $\dot{q}_5^- = 0$, $q_3^- = 18°$ (Immediate sliding)

the impact end condition $v_n^+(Q) = 0$ highly determines the final state $(\mathbf{q}^+, \dot{\mathbf{q}}^+)$ and the total contact impulses (P_n^+, P_t^+) after collision. Thus, one expects that the sensitivity of those results to changes in k_n and χ is low. It is advisable, though, to check such assumption.

For this purpose, we have chosen one of the examples studied above ($\mu = 0.75$, $\dot{q}_5^- = -0.2$ rad/s, $q_3^- = 12°$) as reference case and have proceeded to perturb k_n and χ and compare

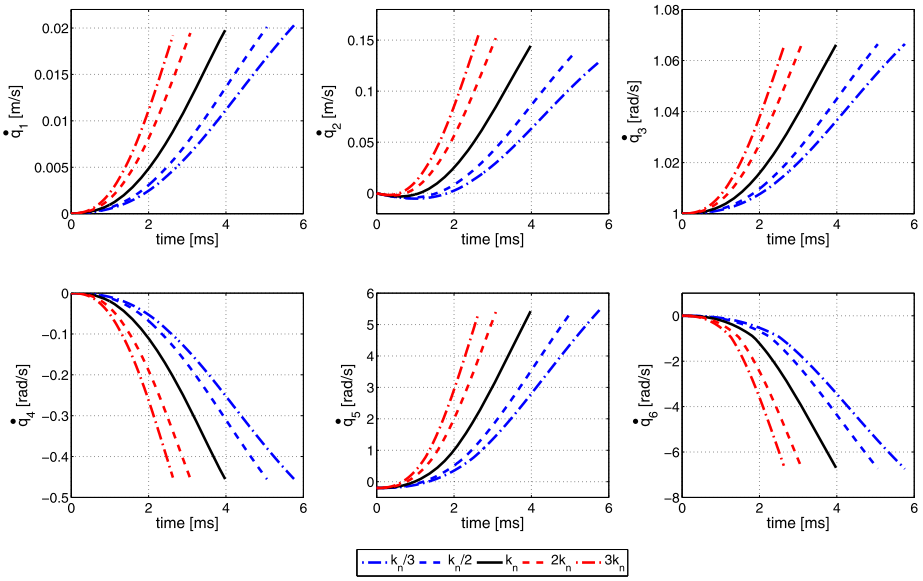

Fig. 18 Evolution of the degrees-of-freedom ($\dot{\mathbf{q}}$) as a function of time for different values of the stiffness parameter k_n

the time evolution and final values of the degrees of freedom $\dot{\mathbf{q}}$ and the contact forces F_n and F_t. This reference case is particularly interesting as it shows a sliding-sticking transition within the impact interval (because for the considered body pose $\mu > \mu_c$). The stiffness and damping parameter values used in this sensitivity study are: $(k_n/3,\ k_n/2,\ k_n,\ 2k_n,\ 3k_n)$ and $(\chi/5,\ \chi/2,\ \chi,\ 2\chi,\ 5\chi)$ where k_n and χ are the nominal parameters used in the previous simulations.

Figures 18 and 19 show the evolution of the six degrees-of-freedom $\dot{q}_i$ for the k_n and χ sets, respectively. As expected, the lower the stiffness and the damping are, the longer the impact duration is. As for the final values of the velocities, the differences are only visible for $\dot{q}_1$ and $\dot{q}_2$. This is logical as they correspond to the components of the swing foot P, which is the farthest point in the kinematic chain from the constrained point Q.

Figures 20 and 21 show the evolution of the contact forces F_n and F_t for the same k_n and χ sets, respectively. The sudden change in F_t corresponds to the sliding-sticking transition, which happens of course independently of the parameter values. The final force values are sensitive to the changes in parameters. Particularly, to that of k_n. However, the total impulses (which is the area under these curves) are very similar as shown in Table 3. Finally, note that the peak force values increase dramatically when increasing the stiffness, but remain similar when the damping is modified. This feature is important in crutch walking, as high contact forces are transmitted to the upper limb joints and may cause damage.

6 Conclusions

In this work, we have presented two different approaches (impulsive and continuous) for the forward dynamics analysis of single-point impact in multibody biomechanical systems. In the first one, the impact condition is established through impulsive bilateral constraints

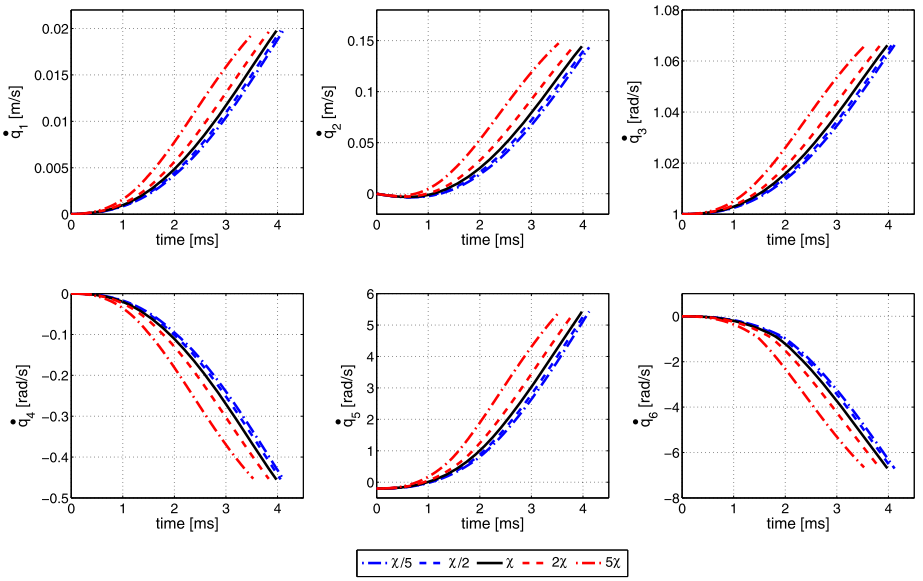

Fig. 19 Evolution of the degrees-of-freedom ($\dot{\mathbf{q}}$) as a function of time for different values of the damping parameter χ

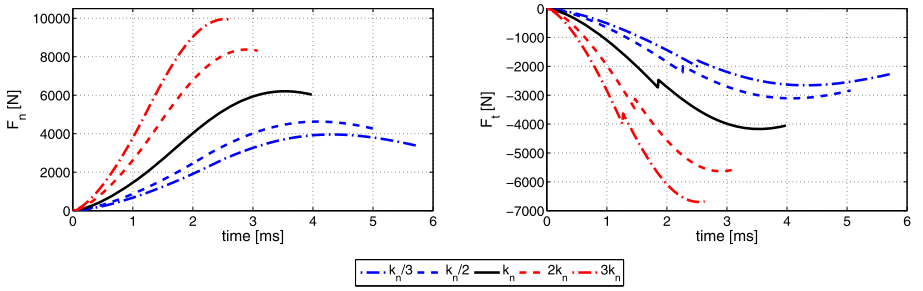

Fig. 20 Evolution of the contact forces (F_n, F_t) as a function of time for different values of the stiffness parameter k_n

and the integrated version of the equations of motion over the impact interval is used. In the second approach, a compliant continuous model is used to define an explicit relationship between the normal contact force and the system state. This model depends on the material properties and the geometry of the bodies in contact. Both approaches assume the Coulomb dry friction model in the tangential direction.

The two approaches yield practically the same results concerning not only the final state, normal and tangential impulses and associated work, but also the P_n-evolution of those variables. Therefore, choosing one or the other will not affect significantly the result of the analysis.

The impulsive approach is advantageous from a calculation point of view as it is all-algebraic. Moreover, it allows the calculation of the critical value of the friction coefficient, thus giving information of the safest system configurations beforehand. We believe that this

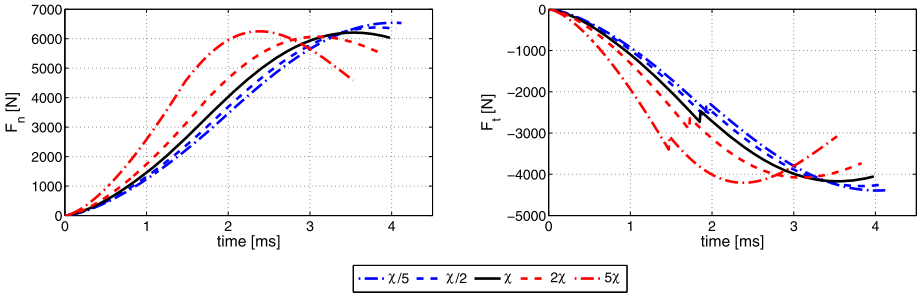

Fig. 21 Evolution of the contact forces (F_n, F_t) as a function of time for different values of the damping parameter χ

Table 3 Total impulses of the contact forces for different values of the contact model parameters

k_n	χ	P_n^+	P_t^+
k_n	χ	14.409 N s	−9.899 N s
$k_n/3$	χ	14.476 N s	−9.927 N s
$k_n/2$	χ	14.461 N s	−9.922 N s
$2k_n$	χ	14.353 N s	−9.868 N s
$3k_n$	χ	14.241 N s	−9.797 N s
k_n	$\chi/5$	14.428 N s	−9.908 N s
k_n	$\chi/2$	14.394 N s	−9.886 N s
k_n	2χ	14.343 N s	−9.858 N s
k_n	5χ	14.331 N s	−9.851 N s

concept can have a potential application in the field of biomechanics. The main drawback of this approach is that no information on the real contact forces can be obtained. On the other hand, the continuous model allows obtaining the value of the ground contact forces, which is relevant for joint damage assessment since those contact forces are transmitted to body joints. From the computational point of view, this approach makes continuity possible in the global methodology to simulate crutch walking (and walking in general), as the problem is always stated through differential equations. An impulsive approach would lead to two different strategies when studying the percussive (or impact) phase and the nonpercussive one.

The results obtained through simulations covering a sufficiently wide set of parameters, configurations and states show that the safest way to crutch walk is attained when keeping an "upright" configuration. From the analyses, it is clear that as the critical friction value μ_c increases when the body leans forward, the most upright configuration is advisable in order to avoid crutch sliding. Furthermore, this configuration leads to higher normal velocity for the foot, thus allowing for a quicker and easier swing phase.

Acknowledgements This work is supported by the Spanish Ministry of Science and Innovation under the project DPI2009-13438-C03-03 and the Natural Sciences and Engineering Research Council of Canada (NSERC). The support is gratefully acknowledged.

References

1. Jaspers, P., Peeraer, L., Van Petegem, W., Van der Perre, G.: The use of an advanced reciprocating gait orthosis by paraplegic individuals: A follow-up study. Spinal Cord **35**, 585–589 (1997)
2. Noreau, L., Richards, C.L., Comeau, F., Tardif, D.: Biomechanical analysis of swing-through gait in paraplegic and non-disabled individuals. J. Biomech. **28**, 689–700 (1995)
3. Requejo, P.S., Wahl, D.P., Bontrager, E.L., Newsam, C.J., Gronley, J.K., Mulroy, S.J., Perry, J.: Upper extremity kinetics during Lofstrand crutch-assisted gait. Med. Eng. Phys. **27**, 19–29 (2005)
4. Slavens, B.A., Bhagchandani, N., Wang, M., Smith, P.A., Harris, G.F.: An upper extremity inverse dynamics model for pediatric Lofstrand crutch-assisted gait. J. Biomech. **44**, 2162–2167 (2011)
5. Thys, H., Willems, P.A., Saels, P.: Energy cost, mechanical work and muscular efficiency in swing-through gait with elbow crutches. J. Biomech. **29**, 1473–1482 (1996)
6. Waters, R.L., Lunsford, B.R.: Energy cost of paraplegic locomotion. J. Bone Jt. Surg., Am. Vol. **67**, 1245–1250 (1985)
7. Shoup, T.E., Fletcher, L.S., Merril, B.R.: Biomechanics of crutch locomotion. J. Biomech. **7**, 11–19 (1974)
8. Opila, K.A., Nicol, A.C., Paul, J.P.: Upper limb loadings of gait with crutches. J. Biomech. Eng. **109**, 285–290 (1987)
9. Malkan, D.H.: Bilateral ulnar neuropraxia: a complication of elbow crutches. Injury: The British Journal of Accident. Surgery **23**, 426 (1992)
10. Donelan, J.M., Kram, R., Kuo, A.D.: Simultaneous positive and negative external mechanical work in human walking. J. Biomech. **35**, 117–124 (2002)
11. Kuo, A.D., Donelan, J.M., Ruina, A.: Energetic consequences of walking like an inverted pendulum: Step-to-step transitions. Exerc. Sport Sci. Rev. **33**, 88–97 (2005)
12. Adamczyk, P.G., Collins, S.H., Kuo, A.D.: The advantages of a rolling foot in human walking. J. Exp. Biol. **209**, 3953–3963 (2006)
13. Van der Spek, J.H., Veltink, P.H., Hermens, H.J., Koopman, B.F.J.M., Boom, H.B.K.: A model-based approach to stabilizing crutch supported paraplegic standing by artificial hip joint stiffness. IEEE Trans. Neural Syst. Rehabil. Eng. **11**, 443–451 (2003)
14. Gilardi, G., Sharf, I.: Literature survey of contact dynamics modelling. Mech. Mach. Theory **37**, 1213–1239 (2002)
15. Stronge, W.J.: Impact Mechanics. Cambridge University Press, Cambridge (2000)
16. Cuadrado, J., Pàmies-Vilà, R., Lugrís, U., Alonso, F.J.: A force-based approach for joint efforts estimation during the double support phase of gait. Proc. IUTAM **2**, 26–34 (2011)
17. Kecskemethy, A.: A novel cylinder-plane foot contact model for human gait motion reproduction. In: Proc. ECCOMAS Thematic Conf. on Multibody Dynamics, Brussels, Belgium (2011)
18. Millard, M., McPhee, J., Kubica, E.: Multi-step forward dynamic gait simulation. In: Bottasso, C.L. (ed.) Multibody Dynamics: Computational Methods and Applications, pp. 25–43. Springer, Berlin (2009)
19. Argatov, I.: Development of an asymptotic modeling methodology for tibio-femoral contact in multibody dynamic simulations of the human knee joint. Multibody Syst. Dyn. (2011, in press). doi:10.1007/s11044-011-9275-6
20. Machado, M., Flores, P., Pimenta Claro, J.C., Ambrósio, J., Silva, M., Completo, A., Lankarani, H.M.: Development of a planar multibody model of the human knee joint. Nonlinear Dyn. **60**, 459–478 (2010)
21. Bei, Y., Fregly, B.J.: Multibody dynamic simulation of knee contact mechanics. Med. Eng. Phys. **26**, 777–789 (2004)
22. Silva, P.C., Silva, M.T., Martins, J.M.: Evaluation of the contact forces developed in the lower limb/orthosis interface for comfort design. Multibody Syst. Dyn. **24**, 367–388 (2010)
23. McGeer, T.: Passive dynamic walking. Int. J. Robot. Res. **9**, 62–82 (1990)
24. Collins, S.H., Wisse, M., Ruina, A.: A three-dimensional passive dynamic walking robot with two legs and knees. Int. J. Robot. Res. **20**, 607–615 (2001)
25. Kuo, A.D.: Energetics of actively powered locomotion using the simplest walking model. J. Biomech. Eng. **124**, 113–120 (2002)
26. Tlalolini, D., Aoustin, Y., Chevallereau, C.: Design of a walking cyclic gait with single support phases and impacts for the locomotor system of a thirteen-link 3D biped using the parametric optimization. Multibody Syst. Dyn. **23**, 33–56 (2010)
27. Hurmuzlu, Y.: Dynamics of bipedal gait: Part I – Objective functions and the contact event of a planar five-link biped. J. Appl. Mech. **60**, 331–336 (1993)
28. Kövecses, J., Kovács, L.L.: Foot impact in different modes of running: mechanisms and energy transfer. Proc. IUTAM **2**, 101–108 (2011)
29. Font-Llagunes, J.M., Kövecses, J.: Dynamics and energetics of a class of bipedal walking systems. Mech. Mach. Theory **44**, 1999–2019 (2009)

30. Carpentier, C., Font-Llagunes, J.M., Kövecses, J.: Dynamics and energetics of impacts in crutch walking. J. Appl. Biomech. **26**, 473–483 (2010)
31. Gilchrist, L.A., Winter, D.A.: A two-part, viscoelastic foot model for use in gait simulations. J. Biomech. **29**, 795–798 (1996)
32. Kaplan, M.L., Heegaard, J.H.: Energy-conserving impact algorithm for the heel-strike phase of gait. J. Biomech. **33**, 771–775 (2000)
33. Winter, D.A.: Biomechanics and Motor Control of Human Movement. Wiley, Hoboken (2005)
34. Batlle, J.A.: Termination conditions for three-dimensional inelastic collisions in multibody systems. Int. J. Impact Eng. **25**, 615–629 (2001)
35. Modarres Najafabadi, S.A., Kövecses, J., Angeles, J.: A comparative study of approaches to dynamics modeling of contact transitions in multibody systems. In: Proc. ASME Int. Design Eng. Tech. Conferences IDETC'05, Long Beach, CA, USA (2005)
36. Agulló Batlle, J., Barjau Condomines, A.: Rough collisions in multibody systems. Mech. Mach. Theory **26**, 656–677 (1991)
37. Batlle, J.A.: The sliding velocity flow of rough collisions in multibody systems. J. Appl. Mech. **63**, 804–809 (1996)
38. Kövecses, J.: Dynamics of Mechanical Systems and the Generalized Free-Body Diagram-Part I: General Formulation. J. Appl. Mech. **75**(061012), 1–12 (2008)
39. Goldsmith, W.: Impact: The Theory and Physical Behaviour of Colliding Solids. Arnold, London (1960)
40. Hunt, K.H., Crossley, F.R.E.: Coefficient of restitution interpreted as damping in vibroimpact. J. Appl. Mech. **42**, 440–445 (1975)
41. Lankarani, H.M., Nikravesh, P.E.: Continuous contact force models for impact analysis in multibody systems. Nonlinear Dyn. **5**, 193–207 (1994)
42. Flores, P., Machado, M., Silva, M.T., Martins, J.M.: On the continuous contact force models for soft materials in multibody dynamics. Multibody Syst. Dyn. **25**, 357–375 (2011)
43. Gonthier, Y., McPhee, J., Lange, C., Piedbœuf, J.C.: A regularized contact model with asymmetric damping and dwell-time dependent friction. Multibody Syst. Dyn. **11**, 209–233 (2004)
44. Dopico, D., Luaces, A., Gonzalez, M., Cuadrado, J.: Dealing with multiple contacts in a human-in-the-loop application. Multibody Syst. Dyn. **25**, 167–183 (2011)
45. Johnson, K.L.: Contact Mechanics, 6th edn. Cambridge University Press, Cambridge (1996)